島根大学地球資源環境学研究報告　22, 93～105 ページ（2003 年 12 月）
Geoscience Rept. Shimane Univ., 22, p.93～105（2003）

Article

Whole-rock analyses of sandstones and mudrocks from the Oshima Belt, Oshima Peninsula, SW Hokkaido

Barry Roser*, Hayato Ueda** and Makoto Kawamura***

Abstract

The Carboniferous –Jurassic Oshima Belt is a Jurassic accretionary complex exposed in the Oshima Peninsula of SW Hokkaido. This report contains whole-rock X-ray fluorescence analyses of 82 turbidite sandstones and mudrocks collected from terrigenous units in the Ohkamotsugawa, Esashi, Kamiiso, and Toi Complexes, which crop out from west to east. The results show the Oshima sandstones are comparatively silica-rich (generally 73-85 wt% SiO_2), and are depleted in CaO, Na_2O, Sr, and ferromagnesian elements (MgO, Fe_2O_3T, Sc, Ni, Cr and V) relative to average upper continental crust. Sandstones and mudrocks form linear trends on oxide/element-Al_2O_3 variation diagrams, typical of sorting fractionation. SiO_2, Na_2O, and to a lesser extent CaO and Sr decrease in abundance as Al_2O_3 increases from sandstone to mudstone, whereas all other elements analyzed except MnO, Sr, and Zr increase in abundance. Elemental abundances in Ohkamotsugawa, Esashi, and Kamiiso sandstones are broadly compatible with derivation from a felsic source. Enrichment of ferromagnesian elements (Fe, Mg, Sc, Ni, Cr, V) in some Toi Complex sandstones are suggestive of a minor mafic to intermediate volcaniclastic component, lending support to the proposed bidirectional source for that unit.

Introduction

The Carboniferous –Jurassic Oshima Belt crops out in patches in the Oshima Peninsula of SW Hokkaido, where it forms the basement for younger volcanic and sedimentary rocks (Kawamura *et al*., 1986). The Oshima Belt comprises one of the Jurassic accretionary complexes of Japan, along with the North Kitakami Belt and the Mino-Tamba terrane, and is considered broadly equivalent to these terranes in its tectonic setting. All are remnants of an arc-trench system which lay along the margin of the Asian continent (Isozaki, 1997).

The Oshima Belt is tentatively divided into five complexes based on geographic distribution, from west to east, the Ohkamotsugawa, Daisengendake, Esashi, Kamiiso and Toi Complexes, respectively (Fig. 1). They consist of complex lithological assemblages, including oceanic volcanic rocks, cherts, limestones, conglomerates, and quartzofeldspathic terrigenous sediments. The latter are considered to have been derived mainly from the continental Asia landmass (Kawamura *et al*. 2000). Such derivation is supported by continental block QFL signatures, high-rank metamorphic detrital garnet compositions, and by 1800-2500 Ma detrital zircon U- Pb ages (Kawamura *et al*., 2000).

The whole-rock geochemistry of clastic sediments is being increasingly used to help constrain source, source area weathering regime, tectonic setting, and terrane

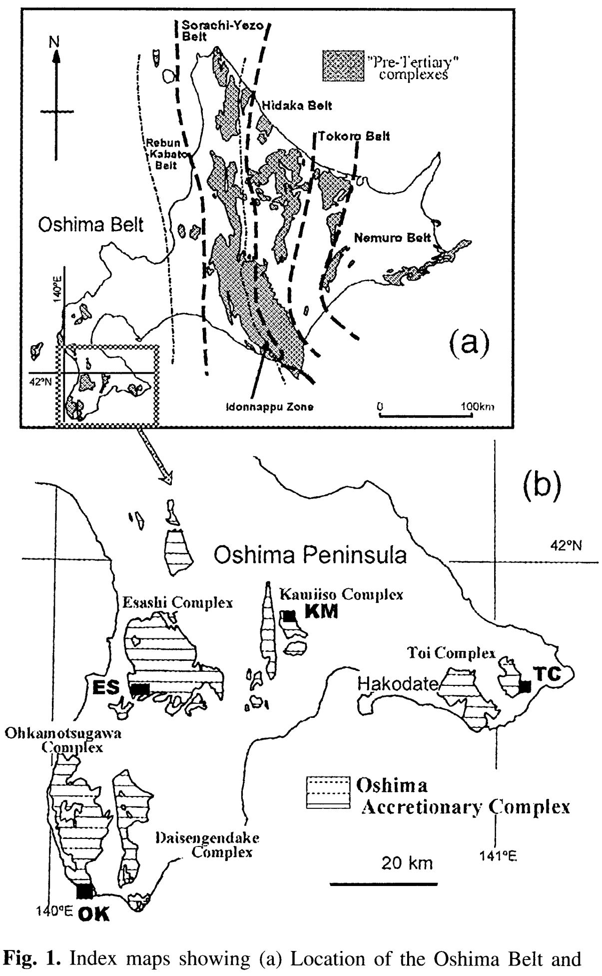

Fig. 1. Index maps showing (a) Location of the Oshima Belt and other pre-Tertiary complexes in Hokkaido, and (b) outcrop of the Oshima Belt in Oshima Peninsula and general location of the sample suites. Adapted from Figure 1 of Kawamura *et al*. (2000).

* Dept. of Geoscience, Shimane University, Matsue 690-8504 Japan
** Dept. of Geology, Faculty of Science, Niigata University, Niigata 950-2181 Japan
***Division of Earth & Planetary Sciences, Graduate School of Science, Hokkaido University, Sapporo 060-0810 Japan

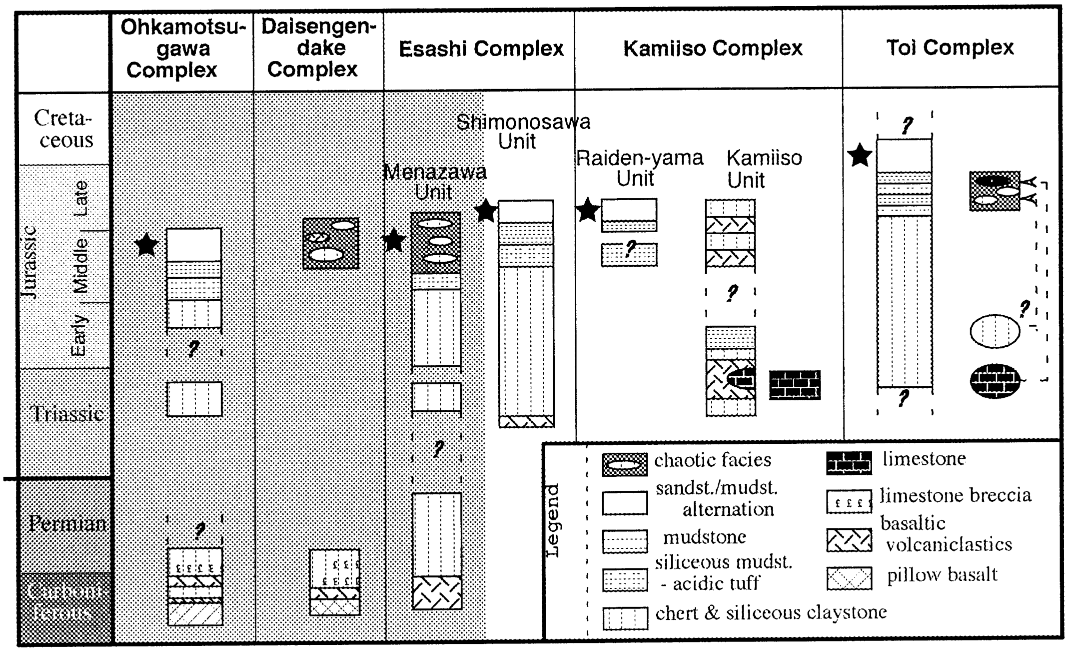

Fig. 2. Tectonostratigraphic organization of the Oshima Belt in Hokkaido, showing position of the suites collected (stars). Adapted from Figure 2 of Kawamura *et al*. (2000).

linkages. At present, the data available for the Oshima Belt is restricted to a small number of major element analyses of sandstones from the Ohkamotsugawa, Esashi, and Kamiiso Complexes (Kawamura *et al*., 2000). In this report, we extend that data with new major and trace element analyses of both sandstones and mudrocks from these three complexes, and also from the Toi Complex. This will allow later comparison with the chemistry of younger terranes to the east (Rebun-Kabato, Idonnappu, Yezo, Tokoro, and Nemuro), as part of a larger project characterizing and examining Hokkaido terranes.

Sample Suites

Four of the five complexes listed above were sampled in this work. The Daisengendake Complex consists of pillow basalt, basaltic volcaniclastics, chert and siliceous claystone, limestone breccia and a chaotic facies, and sampling was thus not considered. Sampling was directed at the terrigenous clastic parts of each complex. The intervals sampled range from upper Middle Jurassic in the Ohkamotsugawa Complex in the west, through to Late Jurassic-earliest Cretaceous in the Toi Complex in the east.

Ohkamotsugawa Complex

The Ohkamotsugawa Complex comprises a Carboniferous to Permian? oceanic assemblage of pillow basalt, basaltic volcaniclastics, limestone breccia, chert and siliceous claystone, plus Triassic and Jurassic cherts and siliceous claystones, siliceous mudstones, mudstones, and late Middle Jurassic sandstone-mudstone alternations (Fig. 2). Samples were collected only from the latter facies, from coastal exposure along Orito Beach. Lithotypes sampled ranged from granule conglomerate (sample OK 1) through medium sandstone (OK 3, 5, 14,), fine sandstone (OK 6, 10, 17) and very fine sandstone (OK 12, 19, 22) to siltstone (OK 2, 9, 15) and mudstone (OK 4, 8, 13, 18, 21). Sampling was confined to coherent sequences showing lateral continuity, generally from midpoints of beds 10-20 cm thick.

Esashi Complex

The Esashi Complex is divided into the Menazawa and Shimonosawa units, both of which were accreted in the Middle to Late Jurassic (Terada and Kawamura, 1997). The Menazawa Unit contains green basaltic volcaniclastics, Permian-Jurassic cherts, Middle to Late Jurassic siliceous claystones and mudstones, and an upper chaotic facies (Fig. 2). Eleven samples (ES 1-11; seven sandstones, four mudstones) were collected from the chaotic facies in the Tomappu River area, mainly from road outcrops.

The base of the Shimonosawa Unit consists of basaltic volcaniclastics, which are succeeded in turn by Triassic-Jurassic cherts and siliceous claystones, siliceous mudstones, mudstones, and finally by alternations of Late Jurassic sandstones and mudstones. It comprises a coherent sequence, multiply stacked by thrust faults (Terada and Kawamura, 1997). Fourteen samples (ES 12-25; ten sandstones; four siltstones and mudstones) were collected from the alternating sandstone-mudstone unit, again from road outcrop.

Kamiiso Complex

The Kamiiso Complex is also divided into two units, the oceanic Kamiiso Unit, and the terrigenous clastic Raiden-yama Unit (Fig. 2). The Kamiiso Unit ranges from Triassic to Late Jurassic in age (Kawamura *et al.*, 2000). It consists of a complex assemblage of limestones, basaltic volcaniclastics, cherts, siliceous mudstones and other oceanic lithotypes interpreted to be of seamount origin (Kawamura *et al.*, 1997). No samples were collected from this unit due to the absence of terrigenous lithotypes.

The Raiden-yama Unit consists of Middle Jurassic siliceous mudstones and Middle to Late Jurassic mudstones and sandstone/mudstone alternations. Nineteen samples were collected (eleven sandstones; eight mudstones), mainly from river-washed outcrops in a traverse along the Hekirichi River to Amemasu Stream. Sandstones occurred mainly in thin (<5 m) packets of amalgamated beds 0.1-0.5 m in thickness, separated by thicker intervals of black mudstone.

Toi Complex

The Toi Complex consists of a chaotic facies (Shirikishinai Unit), which was not sampled, and a quartzofeldspathic terrigenous unit (Karakawa Unit). The Karakawa Unit is floored by Triassic to Middle Jurassic cherts and siliceous claystones, and passes upward into mudstones and Late Jurassic to Earliest Cretaceous sandstone-mudstone alternations (Fig. 2). The Karakawa Unit is distinguished from the terrigenous units of the other complexes by the presence of some cpx-bearing volcaniclastic sandstones. The clinopyroxenes have arc affinities, suggesting that provenance of this unit was mixed and bidirectional, with volcaniclastic detritus supplied from the Rebun-Kabato Belt to the east, and quartzofeldspathic detritus from the west (Kawamura *et al.*, 1997).

Eighteen samples (TC 1-19; thirteen sandstones; five black mudstones) were collected from the alternating sandstone-mudstone part of the sequence, mainly from outcrop along Karakawa Stream and one of its tributaries, near Toi town. The succession sampled was mud-dominated, with sands occurring only as thin isolated beds. Most of the sandstones collected were very fine grained, and many contained thin transposed silt laminae or were disrupted (e.g. TC 13, 15).

Localities for all samples are given in Fig. 3.

Analytical Methods

Samples were chipped to <10 mm maximum diameter using a manual rock splitter. Any chip containing veins or surficial oxidation was discarded after washing in running water to remove loose surface material. The chip was then immersed in deionized distilled water for 24-36 hours, with several changes of water during that time, and subsequently dried at 110℃. The samples were crushed in a tungsten carbide ring mill, in loads of 70-150 g, using maximum mill times of 30-60 seconds. Such mill times are sufficient to produce powders as fine or finer than by agate mortar systems, with no contamination except for tungsten and cobalt (Roser *et al*., 1998; Roser *et al*., 2003). Ten gram subsamples of the resulting pulps were then oven-dried at 110° C for at least 24 hours prior to determination of loss on ignition (LOI).

Gravimetric LOI determinations were made by weighing 5-6 g of dried sample into ceramic crucibles, followed by ignition in an electric furnace at 1000℃ for at least two hours. The ignited material was then manually disaggregated and ground in an agate pestle and mortar, and returned to a 110℃ oven for another 24 hours. This ignited material was then used for preparation of fusion beads for XRF analysis.

Analyses of major elements and 14 trace element were made using a Rigaku RIX-2000 XRF at Shimane University. All analyses were carried out on glass beads prepared in an automatic bead sampler, using an alkali flux comprising 80% lithium tetraborate and 20% lithium metaborate, with a sample to flux ratio of 1:2. Analytical methods, instrumental conditions and calibration follow those described by Kimura and Yamada (1996). Analyses were monitored by repeat analyses of seven GSJ and USGS standards, from new beads not included in the original calibration.

Results

Results are listed in Table 1, reported on a hydrous basis. For all plots and comparisons made here, the data have been recalculated to 100% LOI-free (anhydrous basis). The same normalization factors were also applied to the trace element data.

Major Elements

Silica abundances in the suite vary considerably, from over 90 wt% in two Ohkamotsugawa samples (OK 1, 3) to <60% in the mudstones. SiO_2 shows marked negative correlation with Al_2O_3 (Fig. 4a), as is typical in relatively mature sedimentary suites. Most of the sandstones fall within a narrower range between about 72 and 85% SiO_2 and 9-15% Al_2O_3. Some overlap between sandstones and mudrocks occurs between ~15-18% Al_2O_3, but the two lithotypes are generally chemically distinct (Fig. 4a).

Among the other major elements, TiO_2, Fe_2O_3T, MgO, K_2O, and P_2O_5 are positively correlated with Al_2O_3, and abundances in the sandstones are less than in the mudrocks (Figs. 4b-f, respectively). Strengths of the correlations vary between elements, and there are few consistent differences between the individual suites. Overall abundances of TiO_2 are <1%; Fe_2O_3T <7%; MgO generally <2%; K_2O<7%, and P_2O_5 <0.2% (except for a highly anomalous value of 2.83% in mudstone KM 5, and 0.36% in TC 4). The most significant departures from the trends for these elements are elevated MgO and Fe_2O_3T abundances in a few Toi

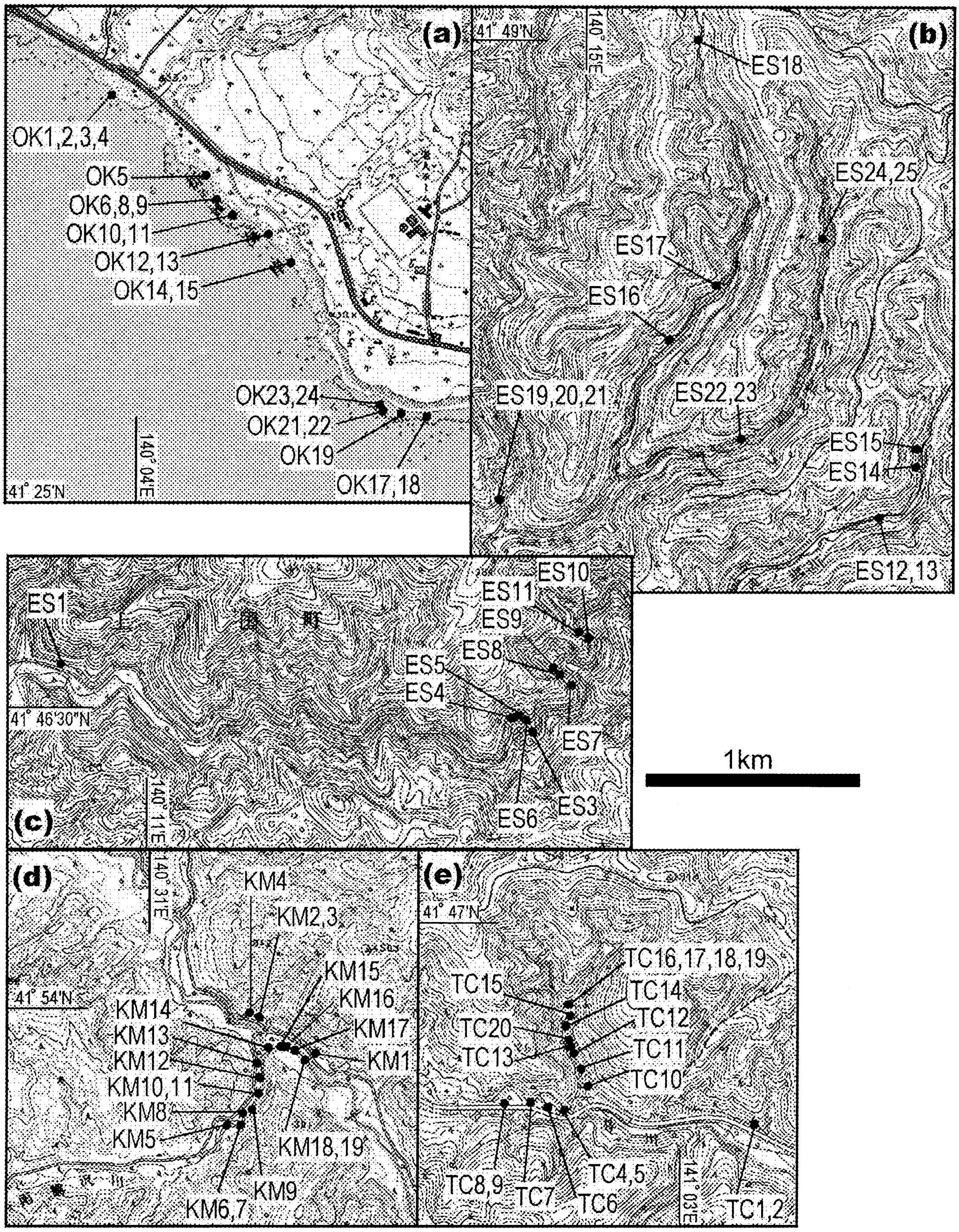

Fig. 3. Sample sites for (a) Ohkamotsugawa Complex; (b) Eshashi Complex, Shimonosawa Unit; (c) Eshashi Complex, Menazawa Unit; (d) Kamiiso Complex; and (e) Toi Complex. Base maps from Geographical Survey of Japan 1/25,000 topographic sheets "Matsumae" (a), "Katsuraoka" (b, c), "Uriyayama" (c), "Jin-ya" (d), and "Kobui" (e).

Complex sandstones (Fig. 4c & d). These two elements also tend to be somewhat lesser in Esashi sandstones compared to those from the Ohkamotsugawa and Kamiiso Complexes.

In contrast to the above group of elements, Na_2O contents show clear negative correlation with Al_2O_3, with abundances falling from ~4% in sandstones to <1% in mudstones (Fig. 4 f). CaO has an almost flat trend, with most samples having low abundances (<0.5 wt%), although a number of sandstones scatter to higher values (Fig. 4h). MnO abundances are all <0.15 wt% (Table 1), and no correlation

Table 1. XRF analyses of sandstones and mudrocks from the Oshima Belt, Oshima Peninsula, Hokkaido. Major elements wt.%; trace elements ppm. SaNr = sample number; Lith = Lithology: Mst = mudstone; zst = siltstone; sst = sandstone (Vf = very fine; F = fine; M = medium; cse = coarse); Gr cgl-granule conglomerate. LOI = Loss On Ignition.

SaNr	Lith	SiO_2	TiO_2	Al_2O_3	Fe_2O_3T	MnO	MgO	CaO	Na_2O	K_2O	P_2O_5	LOI	SUM	Ba	Ce	Cr	Ga	Nb	Ni	Pb	Rb	Sc	Sr	Th	V	Y	Zr
Ohkamotsugawa Complex																											
OK1	Gr cgl	87.68	0.14	4.14	1.38	0.13	0.51	1.04	0.35	1.40	0.06	2.10	98.92	141	38	12	8	4	7	18	80	3.5	85	3.4	10	10	63
OK2	Zst	69.97	0.47	14.78	3.77	0.10	1.16	0.64	1.39	4.67	0.10	2.93	99.98	480	76	31	22	11	18	23	218	10.0	113	15.7	67	22	124
OK3	M sst	90.40	0.14	4.31	0.78	0.06	0.27	0.52	0.79	1.31	0.06	1.11	99.72	220	38	8	7	4	5	12	65	2.2	73	5.7	9	11	97
OK4	Mst	63.94	0.57	17.92	5.04	0.09	1.37	0.40	2.12	5.54	0.19	2.71	99.88	651	81	41	25	15	23	23	237	8.6	127	20.2	89	27	154
OK5	M sst	73.75	0.30	14.13	2.02	0.02	0.49	0.39	3.68	3.52	0.06	1.56	99.92	643	68	12	19	8	4	26	120	4.0	178	12.8	25	16	150
OK6	F sst	74.27	0.35	11.75	2.61	0.06	0.72	1.54	2.42	2.81	0.07	2.75	99.35	520	84	10	15	9	7	18	118	4.2	174	15.4	26	16	243
OK8	Mst	63.89	0.73	18.69	4.57	0.01	1.24	0.18	1.73	5.36	0.11	3.54	100.04	794	81	57	26	15	9	20	228	12.3	80	19.9	119	24	143
OK9	Zst	63.53	0.71	19.06	4.39	0.01	1.23	0.20	1.83	5.57	0.12	3.30	99.95	841	91	49	27	15	10	22	233	12.2	91	21.0	96	23	170
OK10	F sst	72.89	0.18	9.43	1.47	0.13	0.34	4.96	2.67	2.16	0.04	4.77	99.03	364	50	10	12	5	4	23	81	3.5	336	7.8	8	12	95
OK11	Zst-mst	70.56	0.52	15.13	3.48	0.01	0.96	0.19	1.63	4.48	0.11	2.62	99.68	719	70	35	22	12	8	23	193	7.6	103	17.0	66	23	168
OK12	Vf sst	65.47	0.60	17.89	4.42	0.02	1.23	0.24	1.78	5.25	0.14	3.00	100.03	804	80	41	26	14	8	22	222	10.2	112	19.2	82	24	170
OK13	Mst	65.93	0.64	17.55	4.37	0.02	1.27	0.22	2.29	4.71	0.12	3.00	100.11	797	69	56	25	12	9	10	206	10.6	110	19.1	99	18	137
OK14	Med sst	75.22	0.29	12.24	1.45	0.05	0.65	1.05	3.31	2.89	0.05	2.25	99.45	516	83	9	17	10	5	26	111	2.4	194	20.1	18	19	187
OK15	Zst	69.18	0.39	16.63	3.11	0.05	1.02	0.35	1.15	5.21	0.08	2.85	100.02	712	54	24	27	27	10	57	241	7.6	85	24.5	45	38	114
OK17	F sst	83.44	0.17	8.43	0.82	0.07	0.35	0.58	3.07	1.41	0.05	1.37	99.76	274	54	3	10	5	6	18	54	1.4	145	9.5	13	10	175
OK18	Mst	69.54	0.52	15.40	4.28	0.12	1.18	0.65	2.48	3.65	0.10	2.95	100.87	484	68	45	22	11	18	31	161	10.1	141	15.6	76	21	110
OK19	Vf sst	68.74	0.55	16.04	4.19	0.04	1.26	0.31	2.39	3.86	0.12	2.59	100.10	640	72	41	22	12	14	27	172	10.1	100	17.0	81	21	136
OK21	Mst	65.32	0.57	18.13	4.61	0.03	1.28	0.26	2.43	4.60	0.12	2.77	100.12	677	70	47	26	12	15	17	188	9.2	104	17.4	94	21	123
OK22	Vf sst	68.93	0.51	15.58	3.92	0.07	1.13	0.44	1.99	4.21	0.11	2.76	99.65	616	76	33	23	12	16	67	183	7.7	92	17.7	72	21	143
OK23	F sst	80.55	0.20	10.04	1.09	0.05	0.39	0.66	3.44	1.69	0.07	1.54	99.72	307	53	10	13	5	5	29	72	3.2	165	8.1	15	10	107
OK24	F sst	82.00	0.17	9.57	0.83	0.03	0.28	0.30	2.62	2.25	0.05	1.22	99.32	419	52	8	12	5	3	19	93	1.2	134	10.3	6	13	127
Esashi Complex (Menazawa Unit)																											
ES1	Mst	82.35	0.37	7.81	3.08	0.03	0.95	0.16	0.24	2.12	0.11	2.50	99.71	1183	36	31	12	7	17	11	97	7.7	21	5.7	54	16	72
ES3	Med sst	76.22	0.34	11.34	2.06	0.03	0.58	1.22	3.15	2.67	0.06	1.88	99.56	585	75	8	14	6	4	20	81	4.5	202	13.3	25	12	232
ES4	Mst	57.49	0.87	21.41	5.93	0.04	1.66	0.34	1.66	5.85	0.17	4.93	100.35	658	84	61	30	14	16	29	209	14.5	98	21.9	129	25	150
ES5	F sst	78.72	0.30	10.79	1.42	0.03	0.39	0.98	3.49	2.02	0.05	1.43	99.61	427	83	11	13	5	4	17	68	3.0	190	12.2	24	13	217
ES6	VF sst	80.99	0.39	9.48	2.59	0.10	0.77	0.33	1.23	1.99	0.11	2.00	99.97	326	56	28	14	8	12	17	95	7.4	98	9.4	54	16	95
ES7	F sst	74.97	0.32	12.16	1.62	0.06	0.47	1.79	3.43	2.33	0.06	2.19	99.41	401	61	8	16	6	6	19	84	6.1	226	9.7	23	10	172
ES8	Mst	63.01	0.75	18.16	5.55	0.03	1.45	0.23	2.53	3.75	0.18	4.63	100.28	479	77	50	24	12	11	21	145	13.1	96	16.7	98	24	170
ES9	Mst	62.92	0.80	18.80	4.72	0.02	1.43	0.25	2.45	4.15	0.18	4.34	100.07	550	89	56	25	14	8	20	160	15.1	101	19.2	115	24	184
ES10	F sst	74.64	0.36	12.58	2.29	0.03	0.74	1.31	3.69	2.23	0.07	1.86	99.81	520	71	14	16	7	5	17	79	6.5	251	11.9	30	13	215
ES11	F sst	77.28	0.34	11.29	1.96	0.02	0.59	0.76	2.74	2.97	0.06	1.33	99.34	641	73	11	14	7	4	19	92	4.2	186	12.3	26	13	215
Esashi Complex (Shimonosawa Unit)																											
ES12	Sst	77.14	0.29	13.52	0.99	0.00	0.32	0.33	2.68	2.90	0.07	1.60	99.84	515	63	17	17	7	5	26	116	4.8	239	12.7	24	12	167
ES13	Mst	68.18	0.54	17.30	3.25	0.01	0.78	0.19	1.70	4.35	0.11	3.63	100.05	660	66	30	25	14	5	29	180	9.1	202	15.3	74	19	137
ES14	Med sst	76.89	0.26	12.26	1.68	0.06	0.32	0.39	3.09	3.06	0.06	1.75	99.82	621	65	7	15	6	7	19	100	3.5	207	12.1	13	10	157
ES15	VF sst	68.34	0.61	16.86	3.81	0.02	0.87	0.17	1.63	4.53	0.11	3.78	100.74	682	65	38	25	13	5	28	186	9.0	113	15.5	78	19	129
ES16	Zst	66.15	0.63	17.57	4.83	0.06	1.33	0.24	1.23	4.96	0.12	3.01	100.12	675	42	47	25	13	8	18	240	11.7	64	18.4	86	18	135
ES17	F sst	78.08	0.25	12.32	0.64	0.01	0.21	0.34	3.15	3.52	0.06	0.91	99.50	712	53	12	16	6	4	19	110	4.5	211	10.6	19	11	140
ES18	F-med sst	75.53	0.31	13.54	1.53	0.03	0.42	0.43	3.46	2.96	0.07	1.67	99.95	486	75	14	17	7	7	22	102	4.1	248	13.2	24	12	215
ES19	F sst	72.62	0.39	14.83	2.54	0.05	0.53	0.33	2.47	4.15	0.08	1.75	99.73	848	62	16	21	9	4	20	145	5.0	194	13.7	41	15	191
ES20	Med-f sst	79.21	0.28	11.98	0.76	0.02	0.21	0.24	2.53	3.31	0.05	1.09	99.70	689	59	6	16	7	1	17	101	2.7	173	12.6	23	12	194
ES21	Med sst	77.09	0.31	12.79	1.31	0.03	0.28	0.29	2.93	3.48	0.05	1.12	99.70	699	63	14	17	7	2	21	108	3.6	205	12.5	28	12	212
ES22	Med sst	74.40	0.33	13.43	2.36	0.05	0.63	0.58	3.07	3.67	0.08	1.22	99.81	705	62	12	18	8	7	24	131	3.0	262	11.6	24	10	177
ES23	VF sst	71.46	0.47	14.66	2.90	0.03	0.84	0.61	2.89	4.13	0.09	1.89	99.98	695	55	21	20	9	5	22	172	6.3	245	12.0	41	11	169
ES24	Mst	64.06	0.72	17.71	4.74	0.04	1.15	0.31	0.94	4.76	0.16	5.41	99.97	736	69	55	24	14	21	29	195	12.0	119	15.0	105	31	159
ES25	Mst	59.95	0.81	21.22	5.92	0.05	1.40	0.15	0.71	5.99	0.11	4.18	100.49	722	79	67	29	16	17	32	233	17.4	99	20.1	142	35	150

Table 1 (ctd). XRF analyses of sandstones and mudrocks from the Oshima Belt, Oshima Peninsula, Hokkaido.

SaNr	Lith	SiO_2	TiO_2	Al_2O_3	Fe_2O_3T	MnO	MgO	CaO	Na_2O	K_2O	P_2O_5	LOI	SUM	Ba	Ce	Cr	Ga	Nb	Ni	Pb	Rb	Sc	Sr	Th	V	Y	Zr
Kamiiso Complex (Raiden-yama Unit)																											
KM1	F sst	79.17	0.24	10.25	1.76	0.02	0.50	0.60	2.64	2.05	0.04	2.09	99.37	420	64	8	14	6	4	36	88	4.3	95	12.4	15	12	121
KM2	Mst	58.38	0.72	20.85	6.23	0.04	1.40	0.24	1.90	5.28	0.16	4.98	100.19	658	74	52	30	16	22	55	235	12.7	132	22.5	97	24	123
KM3	Mst	62.92	0.73	19.77	3.86	0.02	0.93	0.15	1.40	5.44	0.11	4.31	99.66	670	86	38	30	17	10	40	248	12.0	103	21.4	90	34	170
KM4	M sst	80.03	0.30	10.31	2.12	0.02	0.40	0.20	3.01	1.30	0.05	2.18	99.91	242	72	7	13	6	3	45	66	6.6	142	15.1	22	11	192
KM5	Mst	59.26	0.60	17.32	4.68	0.06	1.10	3.85	1.27	3.99	2.83	3.72	98.66	491	226	38	24	28	17	32	188	14.2	231	18.1	89	25	119
KM6	Med sst	82.00	0.20	9.24	1.98	0.01	0.24	0.22	3.39	0.71	0.04	1.86	99.89	144	50	4	11	5	2	18	38	2.0	127	12.1	17	11	124
KM7	Cse-M sst	81.29	0.22	9.45	2.19	0.01	0.31	0.24	3.27	0.78	0.04	2.00	99.79	165	55	5	11	6	3	20	40	2.5	139	11.6	11	14	137
KM8	M sst	80.74	0.27	10.10	1.67	0.01	0.41	0.30	2.84	1.27	0.05	2.10	99.76	276	54	12	13	6	3	20	60	4.0	122	13.2	24	8	147
KM9	Mst	60.82	0.72	21.54	3.11	0.01	0.66	0.20	1.30	5.89	0.14	5.47	99.85	740	74	38	31	16	10	33	253	10.5	145	24.3	82	18	133
KM10	Mst	62.51	0.70	20.44	2.90	0.01	0.87	0.27	0.30	6.47	0.17	5.09	99.74	728	54	42	30	16	14	25	266	15.9	114	20.5	92	21	146
KM11	Vf sst	72.91	0.40	13.89	3.50	0.02	0.54	0.21	1.65	2.98	0.10	3.53	99.74	403	60	12	19	8	11	26	143	5.3	110	11.2	33	14	179
KM12	Mst	63.96	0.67	20.26	4.03	0.03	0.95	0.18	0.80	4.99	0.11	3.98	99.95	662	67	41	28	15	9	14	230	13.5	86	21.5	89	23	137
KM13	F sst	82.18	0.21	9.84	1.55	0.01	0.33	0.17	1.77	1.39	0.04	2.38	99.87	206	53	10	13	6	4	18	81	2.1	83	11.2	13	9	132
KM14	F sst	75.65	0.32	13.64	2.12	0.01	0.58	0.18	2.91	2.47	0.05	1.88	99.82	528	56	9	18	8	4	20	113	6.0	139	11.3	27	18	135
KM15	M sst	79.03	0.28	10.92	1.89	0.01	0.47	0.21	2.25	2.28	0.04	2.02	99.39	474	61	14	15	7	4	21	93	4.1	92	12.5	25	14	148
KM16	Mst	60.84	0.71	20.63	3.89	0.01	0.87	0.17	1.15	6.68	0.12	4.61	99.66	956	66	47	30	15	5	27	257	11.8	88	20.2	86	17	142
KM17	F sst	79.13	0.28	10.75	1.95	0.01	0.48	0.19	2.36	2.47	0.04	2.08	99.75	494	62	9	14	7	4	22	101	3.9	99	13.2	21	15	163
KM18	Mst	63.01	0.65	19.27	4.16	0.02	0.90	0.25	0.99	5.96	0.15	4.61	99.96	712	75	40	27	16	19	31	247	10.5	78	21.3	72	27	184
KM19	M sst	77.77	0.28	10.71	2.72	0.03	0.60	0.47	2.19	1.96	0.05	2.86	99.63	313	70	8	14	6	6	22	96	4.6	120	13.5	23	14	151
Toi Complex																											
TC1	Mst	67.59	0.62	16.25	4.14	0.04	1.56	0.19	2.11	4.23	0.10	2.89	99.70	661	59	53	22	13	12	14	156	9.9	64	14.5	89	20	191
TC2	F sst	78.41	0.27	11.75	1.85	0.03	0.58	0.31	3.73	1.76	0.05	1.20	99.94	303	52	28	14	7	10	19	68	3.6	167	6.6	26	13	166
TC4	Mst	60.59	0.86	19.63	4.77	0.06	1.72	0.48	1.92	5.74	0.36	3.70	99.85	804	68	66	28	16	17	20	197	15.3	77	18.2	128	29	231
TC5	Vf sst	77.87	0.32	11.61	2.53	0.04	0.83	0.16	2.73	1.96	0.06	1.54	99.66	335	54	32	13	6	8	17	79	4.9	115	7.5	37	12	193
TC6	Vf sst	80.68	0.27	10.70	1.69	0.02	0.54	0.21	3.27	1.37	0.06	1.10	99.91	240	51	37	11	5	7	44	56	2.8	149	6.3	22	10	169
TC7	Vf sst-zst	73.93	0.36	13.18	3.46	0.06	1.14	0.23	2.96	2.22	0.08	2.06	99.67	381	51	35	16	7	18	19	83	5.6	119	7.8	39	12	182
TC8	Mst	58.55	0.88	20.94	5.39	0.06	1.89	0.17	1.62	6.39	0.18	3.85	99.91	917	48	83	29	15	15	28	208	15.2	62	17.8	134	18	213
TC9	F sst	81.75	0.24	9.65	1.91	0.03	0.63	0.20	3.09	1.24	0.05	1.01	99.80	240	49	27	10	5	9	23	49	3.4	160	4.6	17	9	163
TC10	Mst	66.84	0.63	15.68	5.40	0.13	2.00	0.24	1.96	3.63	0.11	3.18	99.79	393	48	60	20	11	34	15	143	11.2	58	12.1	111	19	173
TC11	Mst	65.40	0.65	16.78	5.41	0.10	1.95	0.29	2.59	3.66	0.11	3.03	99.96	605	64	59	23	12	26	33	139	13.0	131	14.4	109	17	167
TC12	Vf sst	78.29	0.24	11.79	2.21	0.03	0.75	0.15	2.80	2.20	0.05	1.47	99.98	387	39	23	14	5	10	17	86	4.8	150	5.8	26	10	121
TC13	Vf sst-zst	55.17	0.59	14.72	6.17	0.11	4.74	5.09	2.39	2.88	0.14	6.80	98.80	483	49	159	17	7	38	20	86	26.2	123	7.1	164	17	115
TC14	F sst	73.73	0.34	11.94	3.03	0.03	1.91	0.85	3.94	1.89	0.06	2.00	99.73	428	47	76	14	6	23	15	47	12.8	156	6.5	60	12	178
TC15	Vf sst-zst	79.73	0.26	9.07	1.97	0.02	0.62	1.67	2.17	1.62	0.05	2.37	99.57	203	64	26	10	6	11	23	67	4.8	90	7.1	22	12	253
TC16	F sst	75.69	0.28	11.34	2.27	0.05	0.98	1.46	3.51	1.79	0.07	2.06	99.50	397	45	45	13	5	18	16	63	6.6	135	5.3	46	10	144
TC17	M sst	66.77	0.41	11.93	4.32	0.06	3.67	2.98	2.39	2.19	0.09	4.55	99.35	558	34	116	14	5	28	13	66	17.7	170	5.3	108	12	137
TC18	M sst	75.19	0.27	11.02	2.67	0.04	1.64	1.49	2.96	2.09	0.04	2.24	99.68	483	37	33	13	5	16	17	61	5.6	146	4.9	45	9	132
TC19	Vf sst	72.18	0.46	13.55	4.30	0.08	1.47	0.44	2.16	2.76	0.08	2.46	99.93	356	54	87	16	7	26	21	109	16.4	65	8.0	89	14	173

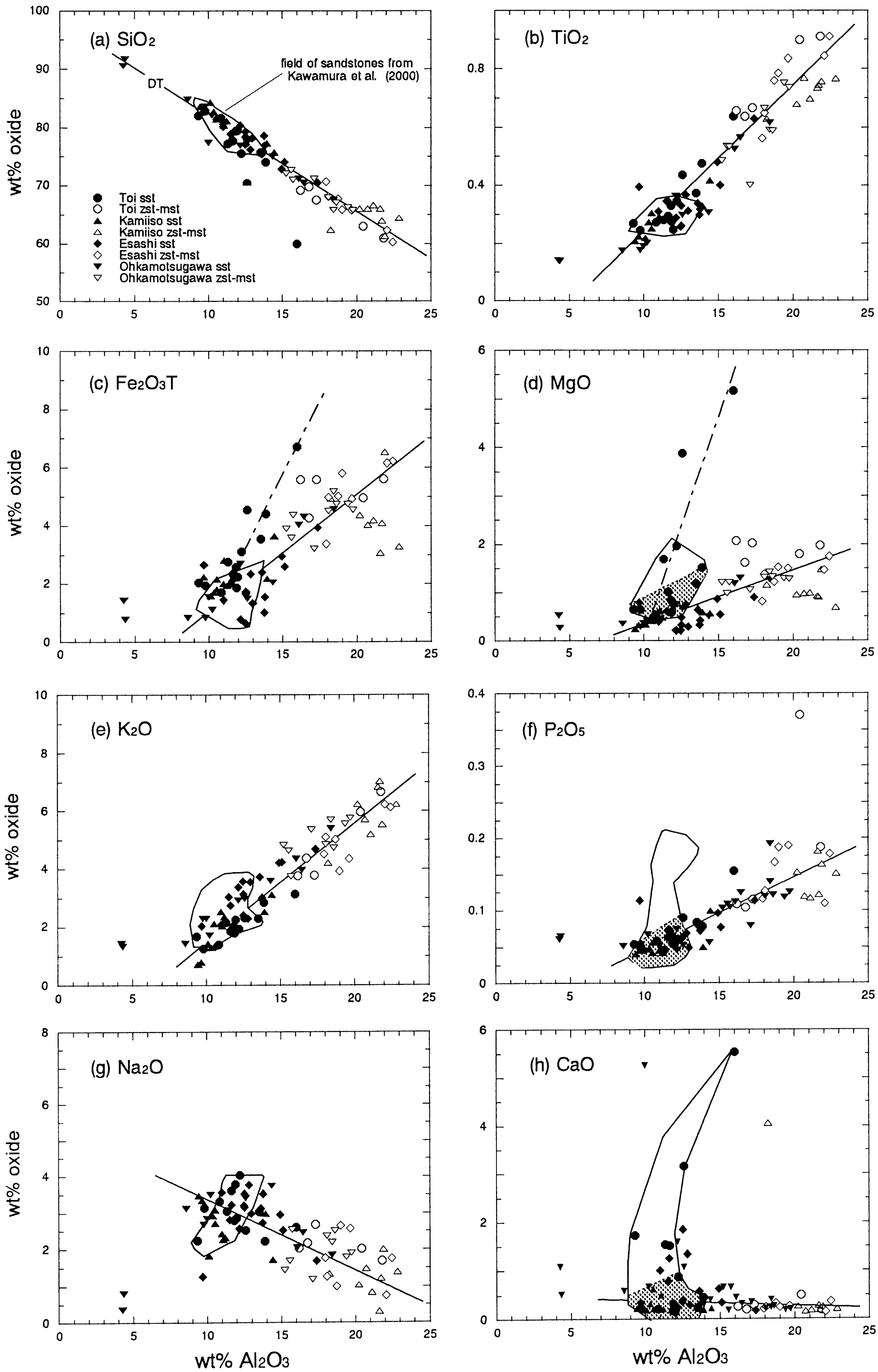

Fig. 4. Major element-Al_2O_3 variation diagrams for the Oshima Belt complexes analyzed, plotted on an anhydrous normalized basis. The fields enclose sandstone data from the Esashi, Kamiiso and Ohkamotsugawa Complexes from Kawamura *et al*. (2000). The MgO field excludes two samples with higher values. Shaded areas within the MgO, P_2O_5 and CaO fields on indicate position of the bulk of their data. Solid lines are illustrative detrital trends (DT) drawn by eye; dashed lines on the Fe_2O_3T and MgO plots indicate enrichment trends in Toi Complex sandstones.

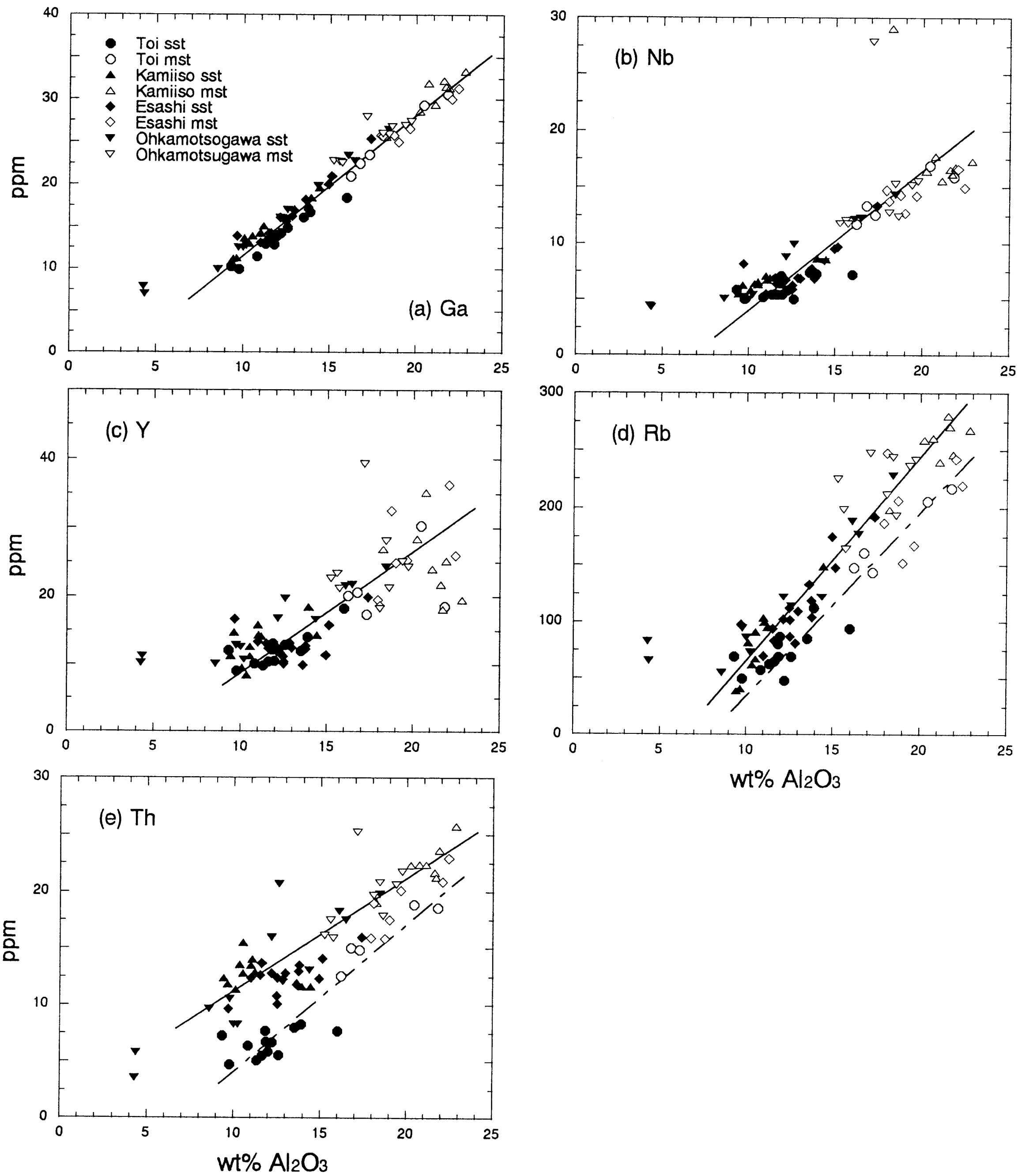

Fig. 5. Ga, Nb, Y, Rb and Th variation diagrams for the Oshima Belt complexes, plotted on an anhydrous normalized basis. Solid lines are illustrative detrital trends drawn by eye; dashed lines on the Rb and Th plots are separate trends in the Toi Complex.

with Al_2O_3 content is evident.

Trace Elements

The trace elements can be divided into four groups based on their behaviour on variation diagrams.

(1) The first group (Ga, Nb, Y, Rb, and Th) show relatively coherent positive correlations with Al_2O_3 content. Gallium abundances range from ~9 ppm in the sandstones to almost 35 ppm in the most aluminous mudstones. Ga also shows the strongest correlation with Al_2O_3, with almost constant Ga:Al ratio in all suites (Fig. 5a) reflecting the close geochemical affinities between these elements. Niobium (5-18 ppm) is also strongly correlated, although abundances in sandstones containing 10-13 wt% Al_2O_3 show rather less variation than do the mudrocks (Fig. 5b). This tendency is also evident for yttrium (7-40 ppm), and abundances in the mudrocks also show greater variability (Fig. 5c). Rb concentrations range from c. 25 ppm to almost 300 ppm (Table 1). Much of the scatter in the Rb data overall is attributable to the Toi Complex samples, which have consistently lower abundances at given Al_2O_3 (Fig. 5d). This pattern is also evident for Th. Abundances in Toi

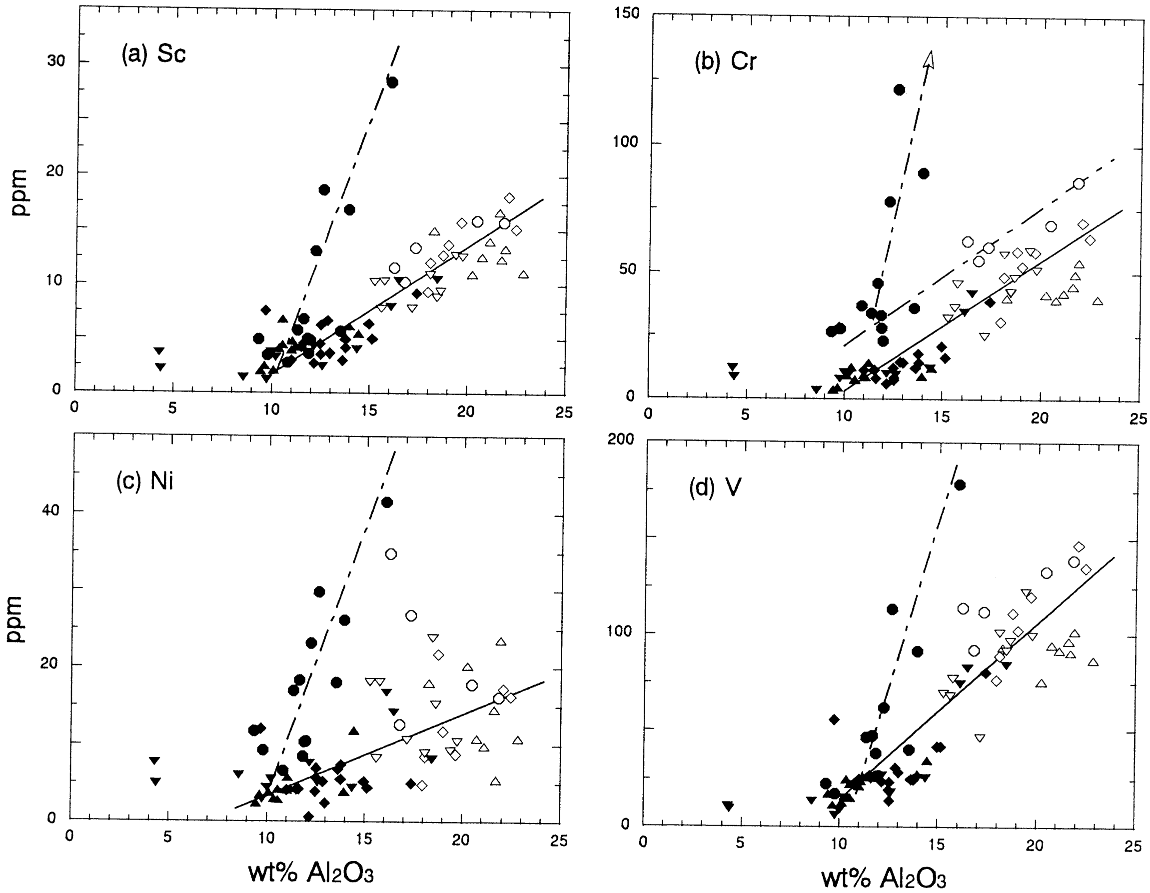

Fig. 6. Sc, Cr, Ni, and V variation diagrams for the Oshima Belt complexes. Solid lines are illustrative detrital trends drawn by eye; dashed lines indicate enrichments or separate trends in the Toi Complex suite. Symbols as in Fig. 5.

sandstones are less than half those in the other suites (Fig. 5e). Although the contrast is less for Toi mudrocks, virtually all contain less Th than their equivalents in the other complexes, and the Toi data overall clearly have different trend.

(2) Four other elements (Sc, Cr, Ni and V) are also positively correlated with Al_2O_3, but are distinguished from the above group by enrichment in some Toi Complex sandstones. For most samples, Sc abundances range from almost zero in the sandstones to ~17 ppm in the most aluminous mudrocks, forming a relatively coherent trend (Fig. 6a). Four Toi sandstones have significantly greater Sc abundances (up to 29 ppm) than other sandstones with similar Al_2O_3 content, and define a separate trend. This is also the case for Cr (Fig. 6b). Cr contents of Ohkamotsugawa, Esashi, and Kamiiso sandstones are low (<10 ppm), whereas those of the mudstones range up to ~75 ppm. The bulk of the data define a positive diffuse trend. In contrast, Toi sandstones have clearly greater Cr contents, with a group at around 20-30 ppm, and higher values ranging up to ~150 ppm. As with Sc, these samples define a separate trend. Abundances are also greater in the Toi mudstones than in the other three complexes, forming a separate but parallel trend that intersects the minimum abundance in Toi sandstones. Nickel contents in the Ohkamotsugawa, Esashi, and Kamiiso Complexes show a general increase with Al_2O_3 up to ~25 ppm, but scatter is considerable (Fig. 6c). As with Cr, Ni abundances in Toi sandstones are almost all greater than their equivalents in the other complexes, with seven samples forming a separate trend up to a maximum of ~40 ppm. Although two Toi mudstones show some enrichment, others do not. A similar pattern is shown by vanadium (Fig. 6d).

(3) Ba, Pb, and Ce show weaker correlation with Al_2O_3, and contrasts in abundances between sandstones and mudstones are not as marked as for the above elements (Fig. 7). Little systematic contrast is evident between the suites, except that Esashi sandstones tend to have greater Ba contents than Toi or Kamiiso sandstones. Ohkamotsugawa Ba values are intermediate. Toi sandstones also have lowest Ce abundances. Sporadic enrichments in Pb above the main trend are spread between the Ohkamotsugawa, Kamiiso and Toi sample suites.

(4) Zr and Sr show poor correlation with Al_2O_3. Zr abundances in the sandstones vary from ~50 to 280 ppm, although most lie in the range 100-220 ppm (Fig. 8a). Abundances in the mudrocks tend to more uniform and are perhaps slightly lower (110-190 ppm) than those in the

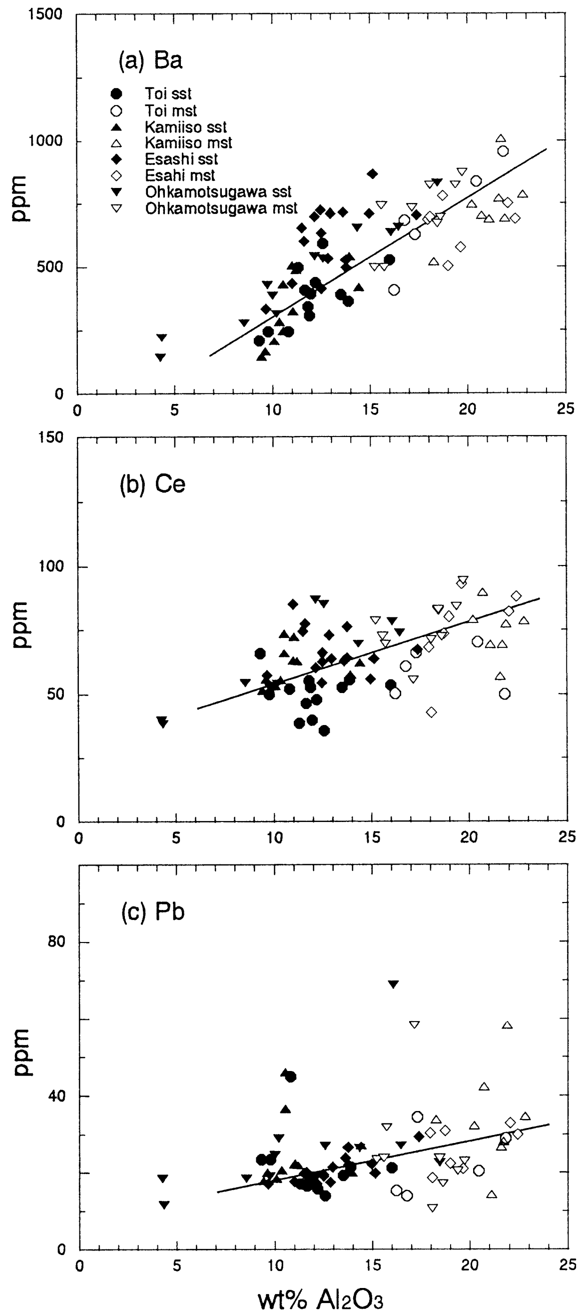

Fig. 7. Ba, Ce and Pb variation diagrams for the Oshima Belt complexes. One Kamiiso mudstone sample (KM 5, anhydrous Ce = 298 ppm) plots well off scale on the Ce plot. This sample also has an anomalous P_2O_5 content (2.98 wt% anhydrous).

sandstones. Little systematic difference is seen between the complexes. Sr abundances in the sandstones are highly variable (generally ~80-280 ppm), but some contrasts are apparent between the suites. Esashi sandstones tend to have the greatest contents, and Kamiiso the least. Many Toi sandstones cluster in an intermediate position, whereas Ohkamotsugawa samples span the compositional spectrum (Fig. 8b). Abundances are generally lesser in the mudrocks, range is restricted (~50-150 ppm), and no clear contrast exists between the suites. Taken overall, Sr abundances decrease slightly as Al_2O_3 increases, although scatter is

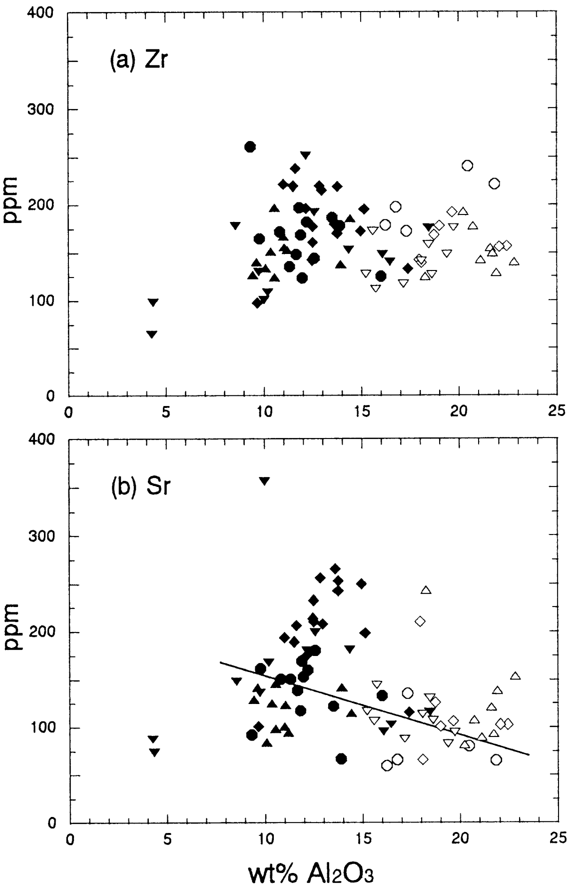

Fig. 8. Zr and Sr variation diagrams for the Oshima Belt complexes. Symbols as in Fig. 7.

considerable.

Discussion

Sandstones and mudrocks from the Oshima Belt display clear contrasts in composition, with the former being less aluminous than the latter. Abundances of other elements also contrast between these end members, leading to systematic and roughly linear trends on oxide and element variation diagrams using Al_2O_3 as the abscissa. Abundances of SiO_2, Na_2O and possibly CaO and Sr decrease as Al_2O_3 increases from sandstone to mudstone. Conversely, TiO_2, Fe_2O_3T, MgO, K_2O, P_2O_5, Ga, Nb, Y, Rb, Th, Sc, Cr, Ni, V, Ba, Pb, and Ce contents increase as Al_2O_3 increases, indicating residence in the clay fraction. These groupings are similar to those observed for quartzofeldspathic sediments suites elsewhere (e.g. Roser, 2000), and reflect separation of quartz, feldspar and felsic lithic fragments from aluminous clays during turbidite deposition. Lack of correlation for Zr and higher concentrations in the sandstones likely reflects concentration in zircon.

Kawamura *et al*. (2000) reported major element data for 27 sandstones from the Ohkamotsugawa, Kamiiso and Esashi Complexes. They stressed the siliceous nature of

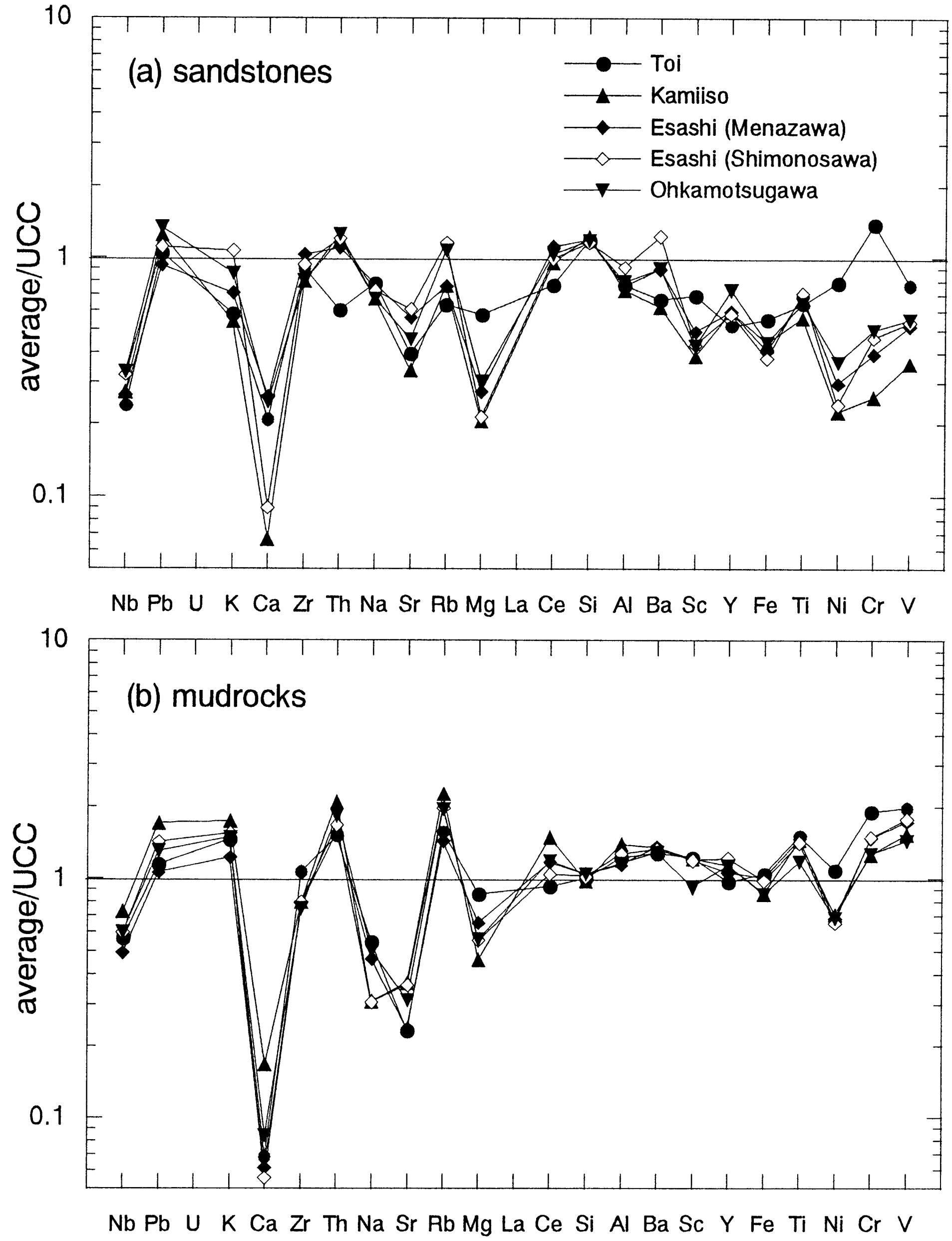

Fig. 9. Average Oshima Belt sandstone (a) and mudrock (b) compositions normalized against the average Upper Continental Crust (UCC) composition of Taylor and McLennan (1985). Elements are arranged from left to right in order of increasing abundance in average Mesozoic-Cenozoic greywacke (Condie, 1993) relative to UCC, following the methodology of Dinelli *et al.* (1999). Major elements are normalized using their oxide values (wt%), and trace elements using ppm abundances. The Ohkamotsugawa average excludes granule conglomerate OK 1.

these rocks (average 79.4 wt%), and noted that this was a common characteristic of Japanese Jurassic accretionary terranes. The relatively siliceous nature of Oshima sandstones is confirmed by our new data, with anhydrous SiO_2 contents mostly lying between 75 and 85 wt%. Toi Complex sandstones are also shown to be relatively siliceous (mostly 74-83% SiO_2 anhydrous). In general, the major element compositions of the Oshima sandstones analyzed here are comparable with those reported by Kawamura *et al*. (2000), with most falling within the fields of that study (Fig. 4). Although P_2O_5, CaO, and MgO trend across the lower parts of their respective fields, most of the data reported by Kawamura *et al*. (2000) also lie in those areas.

The mature nature of the Oshima sandstones is well illustrated by multi-element plots of their average compositions, normalized against average Upper Continental Crust (UCC), as shown in Fig. 9a. Ohkamotsugawa, Kamiiso and Esashi (Menazawa and Shimonosawa) averages show remarkably similar shapes, with near-crustal abundances of

Pb, K_2O, Zr, Rb, Al_2O_3 and Ba, and slight enrichments of Th, Ce, and SiO_2. In contrast, CaO, Na_2O, Sr, and MgO are strongly depleted, and abundances of the mainly ferromagnesian elements in the segment Sc-V decrease from left to right. These features are symptomatic of derivation from a felsic source, further modified by destruction of feldspar during source area weathering. The multi-element plot of the mudrock averages (Fig. 9b) shows much closer coherence to UCC composition, especially in the segment MgO to V. Depletion in CaO, Na_2O and Sr is greater and more uniform than in the sandstones.

The sandstone multi-element plot (Fig. 9a) also highlights a small difference in the composition of Toi Complex sandstones overall compared to the other suites, despite similar SiO_2 contents. The Toi sandstone average has lower Th and Ce, and comparative enrichment in the ferromagnesian elements MgO, Sc, Fe_2O_3T, Ni, Cr and V, reflecting the higher concentration of these elements in some samples identified on the variation diagrams (Figs. 4 and 6). This pattern is also evident for MgO, Ni, Cr, and V in the mudrocks, although the contrast is less (Fig. 9b). This association of elements is suggestive of a minor mafic or intermediate volcaniclastic component, supporting the concept of a mixed source for the Toi Complex, as proposed by Kawamura *et al*. (1997). In contrast, the more uniform composition and elemental abundances of the Ohkamotsugawa, Kamiiso and Esashi complexes support derivation from a felsic source in continental Asia. A more detailed assessment of geochemical provenance signatures in the Oshima Belt will be made in a future publication.

Conclusions

Oshima Belt sandstones are relatively silica-rich, and have elemental abundances compatible with derivation from a felsic source. Traditional variation diagrams show that SiO_2, Na_2O, and to a lesser extent CaO and Sr decrease in abundance as Al_2O_3 increases from sandstone to mudstone, whereas all other elements analyzed except MnO, Sr, and Zr increase in abundance. Compositions of the Ohkamotsugawa, Esashi, and Kamiiso Complexes are very similar, suggesting a common source. Sporadic enrichments of ferromagnesian elements (Fe, Mg, Sc, Cr, Ni and V) in Toi Complex sandstones suggest presence of a mafic to intermediate volcaniclastic component which is absent from the three complexes to the west. This lends support to the concept of a bidirectional, mixed source for the Toi Complex.

Acknowledgements

This work was supported by Monbukagakusho grant-in-aid 13440147 (to B.P.R.).

References

Condie, K. C. 1993. Chemical composition and evolution of the upper continental crust: Contrasting results from surface samples and shales. *Chem. Geol*., **104**, 1-37.

Dinelli, E., Lucchini, F., Mordenti, A. and Paganelli, L. 1999. Geochemistry of Oligocene-Miocene sandstones of the northern Apennines (Italy) and evolution of chemical features in relation to provenance changes. *Sed. Geol*., **127**, 193-207.

Kawamura, M., Tajika, J., Kawamura, T. and Kato, Y. 1986. Constitution and occurrences of the Paleozoic and Mesozoic formations in S.W. Hokkaido, northern Japan. *Monograph Assoc. Geol. Collab. Japan*, **31**, 17-32.*

Kawamura, M., Ozawa, S., Kameyama, S. and Iwata, K. 1997. Supplemental data for the Kamiiso and Toi Complexes of the east Oshima Belt, SW Hokkaido. *In*: Kawamura, M., Oka, T. and Kondo, T. (eds.) *Commem. Vol, Prof. M. Kato*, pp. 111-120.*

Kawamura, M., Yasuda, N., Watanabe, T., Fanning, M. and Terada, T. 2000. Composition and provenance of the Jurassic quartzofeldspathic sandstones of the Oshima Accretionary Belt, SW Hokkaido, Japan. *Memoirs Geol. Soc. Japan*, **57**, 63-72*.

Kimura, J.-I. and Yamada, Y. 1996. Evaluation of major and trace element analyses using a flux to sample ratio of two to one glass beads. *Jour. Mineral. Petrol. Econ. Geol*., **91**, 62-72.

Isozaki, Y. 1997. Jurassic accretion tectonics of Japan. *The Island Arc*, **6**, 25-51.

Roser, B.P. 2000. Whole-rock geochemical studies of clastic sedimentary suites. *Memoirs Geol. Soc. Japan*, **57**, 73-89.

Roser, B.P., Sawada, Y. and Kabeto, K. 1998. Crushing performance and contamination trials of a tungsten carbide ring mill compared to agate grinding. *Geoscience Reports of Shimane University*, **17**, 1-11.

Roser, B.P., Kimura, J.-I. and Sifeta, K. 2003. Tantalum and niobium contamination from tungsten carbide ring mills: much ado about nothing. *Geoscience Reports of Shimane University*, **22**, (this volume).

Taylor, S. R. and McLennan, S. M. 1985. *The continental crust: its composition and evolution*, Blackwell Scientific, Oxford.

Terada, T. and Kawamura, M. 1997. Geology of the Esashi Complex, Oshima Belt, SW Hokkaido - an imbricated stack of tectonic slices. *In*: Kawamura, M., Oka, T. and Kondo, T. (eds.) *Commem. Vol, Prof. M. Kato*, pp. 243-250.*

* In Japanese, English abstract.

(Received: Nov. 21, 2003, Accepted: Dec. 12, 2003)

（要　旨）

バリー・ロザー・上田勇人・川村信人，2003，西南日本ほか軌道，渡島半島，渡島帯の砂岩と泥質岩の全岩分析，島根大学地球資源環境学研究報告，22, 93-105.

石炭系－ジュラ系渡島帯はジュラ紀の付加帯で，北海道渡島半島に露出する．本研究では渡島帯大鴨津川，江差，上磯，戸井コンプレックスのタービダイト堆積物の砂岩と泥質岩 82 試料の XRF 全岩化学組成分析を報告する．渡島帯砂岩の化学組成は全体的に SIO_2 に富み(73–85 wt.%)，平均的上部地殻組成に比較して CaO，Na_2O，Sr や苦鉄質元素に乏しい．砂岩と泥質岩は Al_2O_3–酸化物図で直線的な化学トレンドを示し，典型的な粒度分化を示す．大鴨津川，江差，上磯コンプレックスの砂岩は全体的に酸性の起源岩に起因することを示している．戸井コンプレックスの砂岩は少量の中性－塩基性成分の付加を示しており，二方向流による砕屑物の供給があったという提案を支持している．